AIAA JOURNAL
Vol. 34, No. 4, April 1996

Boundary-Layer Transition on Swept Cylinders at Hypersonic Speeds

Akira Murakami*
National Aerospace Laboratory, Chofu, Tokyo 182, Japan
and
Egon Stanewsky† and Paul Krogmann‡
DLR, German Aerospace Research Establishment, Göttingen D-37073, Germany

We present boundary-layer transition data on swept cylinders in hypersonic flow that were obtained in the hypersonic Ludwieg-tube wind tunnel of DLR. Experiments were conducted at M_∞ = 5.0 and 6.9 for three swept cylinders with and without end plates and sweep angles of 30, 45, and 60 deg, respectively. To determine the state of the boundary layers, the liquid-crystal technique was applied. In addition, the response of attachment-line transition to surface roughness heights due to trip wires for sweep angles of 45 and 60 deg at M_∞ = 5.0 was investigated. Freestream Reynolds numbers based on cylinder diameter for attachment-line transition were about 0.2–0.3 × 10^6 for the end plate disturbances and 0.9–1.2 × 10^6 for no contaminations. Trends of attachment-line transition Reynolds numbers with surface roughness heights are roughly similar to subsonic ones with respect to critical roughness heights. The behavior of the attachment-line transition around the critical roughness heights, however, depended strongly on spanwise Mach numbers. With flow visualizations, off-attachment-line transition could be observed, as well as fine streak pattern in laminar flow region upstream of the transition front, confirming streamwise vortices induced by crossflow instability at hypersonic speeds.

Nomenclature

D = cylinder diameter
d = diameter of trip wires
g = nondimensional spanwise velocity, v/ve
H = ratio of local Reynolds number to freestream Reynolds number
h = nondimensional static enthalpy, $CpT/CpTe$
M = Mach number
Q = resultant velocity
R = local Reynolds number based on boundary-layer length scale
ReD = freestream Reynolds number based on cylinder diameter
$Re\theta$ = local Reynolds number based on laminar momentum thickness at attachment line
s = spanwise distance from upstream tip of cylinder
T = temperature
U = velocity component normal to cylinder leading edge
u = chordwise velocity component in boundary layer
V = spanwise velocity component
v = spanwise velocity component in boundary layer
w = crossflow velocity component in boundary layer
x, y, z = coordinates; see Fig. 3
β = nondimensional crossflow velocity, w/Qe
γ = specific heat ratio
Δ = normal distance from model surface to the point of $0.01w_{\max}$
δ_s = calculated attachment-layer thickness
ζ = nondimensional distance from wall, $\rho/\rho_e \cdot z/\eta$
η = boundary-layer length scale, $[\nu/(\mathrm{d}ue/\mathrm{d}x)_{x=0}]^{0.5}$
θ = laminar boundary-layer momentum thickness or chordwise angular coordinate from attachment line
Λ = sweep angle
λ = wave length of crossflow vortices
ν = kinematic viscosity
ρ = density
χ = local crossflow Reynolds number

Subscripts

crit = critical roughness height
e = edge of boundary layer
es = edge of attachment layer
max = maximum value
r = recovery temperature
t = boundary-layer transition
w = wall condition at attachment line
δ = boundary-layer thickness
∞ = freestream conditions upstream of bow shock
0 = isentropic stagnation conditions

Superscript

$*$ = parameter evaluated at a reference temperature

Introduction

THE understanding and prediction of boundary-layer transition at hypersonic speeds is very important for the successful development of hypersonic vehicles with regard to thermal protection, drag, and engine inlet design. To understand the transition phenomena and to establish reliable prediction methods, detailed experimental investigations are required, as well as theoretical ones. But there are few experimental data at hypersonic speeds especially for highly three-dimensional boundary layers as in the leading-edge region of swept wings.

It is well known that transition in the leading-edge region of swept wings at subsonic speeds is caused by two distinct mechanisms. The first one is called attachment-line contamination. Here, attachment layers are contaminated by disturbances generated in the vicinity of the fuselage/wing junction and/or surface roughness on the attachment lines. Consequently, attachment-line transition occurs and the

Received April 18, 1995; presented as Paper 95-2276 at the AIAA 26th Fluid Dynamics Conference, San Diego, CA, June 19–22, 1995; revision received Aug. 25, 1995; accepted for publication Aug. 31, 1995.

*Senior Researcher, Aeroengine Division, 7-44-1 Jindaijihigashimachi. Member AIAA.
†Head, High Speed Aerodynamics Branch, Institute for Fluid Mechanics, Busenstraße 10. Member AIAA.
‡Scientist, Institute for Fluid Mechanics, Bunsenstraße 10. Member AIAA.

boundary layer on the entire wing surface becomes turbulent. The second mechanism is crossflow instability. The boundary layers at the locations off the attachment line of swept wings are highly three dimensional due to the prevailing pressure gradients, and crossflow is produced within the boundary layers. The crossflow velocity profile has at least one inflection point that introduces instability to small disturbances. Both mechanisms are expected to cause the boundary-layer transition near the leading edge of swept wings at relatively low Reynolds numbers.

Poll[1–3] studied this problem at subsonic speeds and correlated the attachment-line transition behavior with two parameters: the attachment-line similarity parameter $\bar{R} = V_{es}\eta/\nu$ and the ratio of roughness heights (e.g., trip wire diameter) to local length scale d/η. Poll extended the attachment-line transition correlation supersonic speeds by introducing the compressible similarity parameter $\bar{R}^* = V_{es}\eta^*/\nu^*$ evaluated at a reference temperature. He[1–3] correlated the available data at that time with this parameter and showed that $\bar{R}^* = 245$ gave the conditions necessary for the onset of transition caused by large upstream contaminations (e.g., end plates). Bushnell and Huffman[4] previously correlated a large amount of data at super-/hypersonic speeds. They showed that the attachment-line transition occurred at about $ReD = 0.2 \times 10^6$ for large upstream disturbances, but for no disturbances, it did not occur up to $ReD = 0.8 \times 10^6$, which was the upper limit for the available data at that time. Recently, Creel et al.[5] experimentally studied boundary-layer transition on swept circular leading edges at Mach 3.5 using the low-disturbance wind tunnel at NASA Langley Research Center. They particularly investigated the effects of tunnel noise level on transition and showed that without trip or end plate disturbances, the attachment-line transition occurred at $ReD = 0.7$–0.8×10^6 ($\bar{R}^* = 650$–700) independent of tunnel noise levels, but with a small trip on the attachment line, transition Reynolds numbers were reduced by high tunnel noise. They[5] observed crossflow vortices downstream of attachment lines for laminar boundary-layer flows at supersonic speeds in oil-flow studies, and also showed that transition off attachment lines without trip or end plate disturbances occurred at about the same Reynolds numbers as on the attachment lines. Arnal et al.[6] studied boundary-layer tripping due to roughness elements at hypersonic speeds. Their results showed that for large roughness elements on the attachment-line Poll's criterion[1–3] was valid, and they concluded that Poll's criterion could be applied for several types of gross disturbances, e.g., end plates and tripping devices. They[6] also investigated effects of roughness elements placed at locations off the attachment line on transition and found that it was more difficult for the roughness elements off the attachment line to cause the boundary-layer transition than on the attachment line.

As shown in previous investigations, transition phenomena on swept wings are very complex, and more experimental data are required at hypersonic speeds to understand the phenomena. We are, therefore, focusing part of our research on the boundary-layer transition near the leading edge of swept cylinders at hypersonic speeds. The objective of our research is to identify the transition process due to attachment-line contamination and/or crossflow instability at hypersonic speeds and to determine the effects of Mach numbers and surface roughness heights on the transition Reynolds numbers and the validity of previous criteria. In the present study, boundary-layer transition on swept cylinders at hypersonic speeds was experimentally investigated with liquid-crystal flow visualizations.

Experiments

Test Facility

Experiments were carried out in the Ludwieg-tube wind tunnel of DLR (RWG). The facility has three tubes for freestream Mach numbers of 3–4, 5–7, and 9–12, respectively. In the present study, the tube for $M_\infty = 5$–7 was used. The diameter of the test section is 0.5 m. The stagnation condition prevailing behind the expansion wave, traveling in the storage tube after the fast-acting valve has been opened, is nearly constant until the expansion wave reflected at the closed end of the tube again reaches the nozzle throat. The variation of the stagnation condition during the wind-tunnel run is of the order of less than 1%. The run time is about 0.3 s that corresponds to the time of the expansion wave traveling twice the tube length of 80 m. A detailed description of the facility is given in Ref. 7. Normalized fluctuations of pitot pressure and mass flow in the freestream of the test section at $M_\infty = 5.0$, which were measured by Wendt et al.,[8] are given in Fig. 1. For the Reynolds number range of the present experiments, the pitot pressure fluctuations are 1.2–1.8%, and the mass flow fluctuations are 1.1–1.6% of their corresponding mean values. This flow quality is fairly good compared to conventional hypersonic wind tunnels not designed to establish quiet flow conditions.

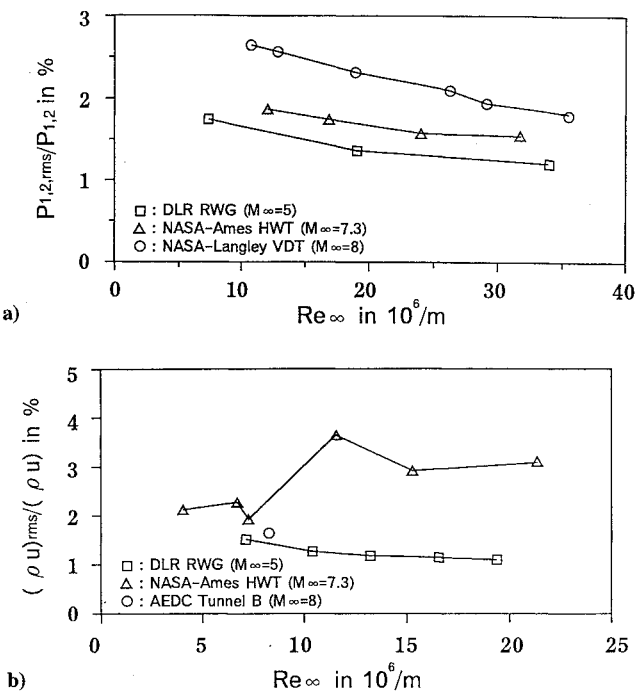

Fig. 1 Freestream noise level of Ludwieg-tube wind tunnel at $M_\infty = 5.0$: a) normalized pitot pressure fluctuations and b) normalized mass flow fluctuations.

Models

Experimental models were three cylinders with sweep back angles of $\Lambda = 30$, 45, and 60 deg, respectively. The diameter of the cylinders was $D = 40$ mm and the span was 300 mm. A fairing cover could be attached on the leeward side of the cylinders. The fairing shape was designed to give a continuity of surface slope at the maximum thickness location. Sharp leading-edge end plates parallel to the freestream direction could be attached at both ends of the cylinders. The form of their leading edge was semicircular and the distance between the leading edge and the attachment line of the cylinders was 40 mm for each model. A sting fixed at the midspan supported the model. In the experiments for surface roughness effects, tripping wires were attached at the location of $s_{trip} = 200$ mm ($s_{trip}/D = 5$) from the upstream tip of the cylinders. The material of the cylinders was Plexiglas®, which was one of the low heat conducting materials that gave a good spatial resolution for thermal imaging obtained by the liquid-crystal technique. The models, after blackening, were sprayed with microcapsulated thermocromic liquid crystals. The measured surface roughness was 14 μm, approximately corresponding to the diameter of the microcapsules. A sketch of the model with $\Lambda = 45$ deg is shown in Fig. 2. Notation and surface coordinate system used in the present study is shown in Fig. 3.

Liquid-Crystal Technique

In the present study, the liquid-crystal technique was applied to determine the state of the boundary layer. The apparent color of microencapsulated thermocromic liquid crystals changes from red to blue with increasing temperature, and the process is reversible. From the color change of the liquid crystals coated on the model during the wind-tunnel run, heat transfer rates at the wall of the

Table 1 Test conditions

M_∞	Λ, deg	M_{es}	$ReD \times 10^6$	$Re\theta$	$\bar{R}^*$	T_0, K	T_w/T_0	Note
5.0	30	1.15	0.17–0.49	100–172	217–369	535	0.55–0.66	end plate
5.0	45	1.89	0.28–1.17	179–366	353–721	400	0.73–0.81	trip wire
5.0	45	1.89	0.15–0.30	149–208	284–398	570	0.51–0.62	end plate
5.0	60	2.89	0.37–1.04	284–478	444–746	400	0.73–0.81	trip wire
5.0	60	2.89	0.16–0.62	205–400	319–623	560	0.52–0.63	end plate
6.9	45	2.03	0.17–0.24	123–147	232–276	500	0.59–0.65	end plate
6.9	60	3.25	0.11–0.30	144–245	206–351	540	0.55–0.60	end plate

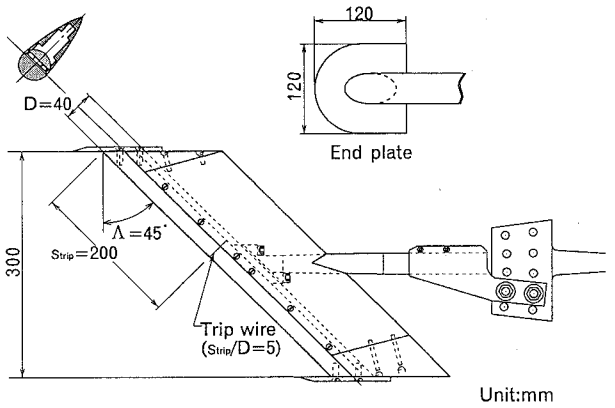

Fig. 2 Sketch of a Λ = 45 deg cylinder model.

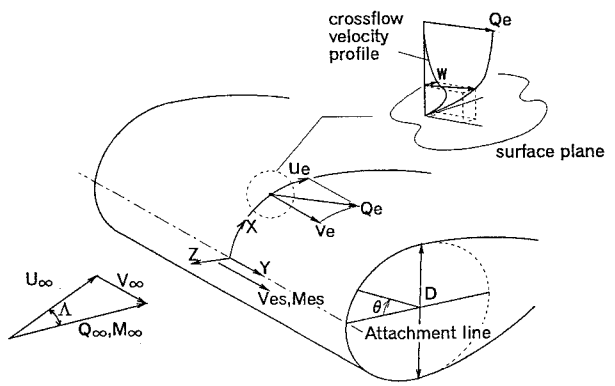

Fig. 3 Notation and surface coordinate.

model can be obtained. Since the heat transfer rates depend on the state of the boundary layer, it is easy to determine the transition. Details of the technique are given in Ref. 9.

The model sprayed with liquid crystals was installed horizontally in the wind tunnel and was illuminated by a slide projector. The color change of the liquid crystals during a wind-tunnel run was recorded by a video recorder at the rate of 50 frames/s.

Test Conditions

Test conditions are given in Table 1. The experiments were conducted at freestream Mach numbers of $M_\infty = 5.0$ and 6.9. Since the stagnation temperature T_0 was held constant during each test case, the freestream Reynolds number was controlled by the stagnation pressure. The ratio of wall to stagnation temperature T_w/T_0 was approximately 0.7–0.8 for the lower stagnation temperature ($T_0 = 400$ K) and 0.5–0.7 for the higher one ($T_0 \geqq 500$ K).

Transition Correlation Parameters

Attachment Line Parameters

In the present study, a spanwise Mach number at the attachment line and two kinds of Reynolds numbers that are based on the laminar momentum thickness and the local length scale, respectively, are used for attachment-line transition to make it easy to compare with previous results. The following are the definitions of these parameters and the formulas used to calculate them in the present study. Values of these parameters for the present test conditions are shown in Table 1.

The spanwise Mach number at the attachment line, M_{es}, can be calculated by the following equation if assuming a plane shock wave parallel to the attachment line:

$$M_{es} = \frac{M_\infty \sin\Lambda}{\sqrt{1 + [(\gamma - 1)/2]M_\infty^2 \cos^2\Lambda}} \tag{1}$$

The local momentum thickness Reynolds number $Re\theta = V_{es}\theta/\nu_{es}$ is calculated from the following relation with the freestream Reynolds number based on the cylinder diameter $ReD = Q_\infty D/\nu_\infty$:

$$Re\theta = \sqrt{ReD} \times \sqrt{\left[\sin\Lambda \tan\Lambda \Big/ \left(\frac{D}{U_\infty}\frac{du_e}{dx}\right)_{x=0}\right]}$$

$$\times \sqrt{\frac{\nu_\infty}{\nu_{es}}} \int_0^{\zeta_\delta} g(1-g)\,d\zeta \tag{2}$$

where $\int g(1-g)\,d\zeta$ is the spanwise momentum integral that can be obtained by laminar boundary-layer theory. A nondimensional chordwise velocity gradient $(D/U_\infty \cdot du_e/dx)_{x=0}$ is calculated assuming the modified Newtonian pressure distribution.

The local length scale Reynolds number proposed by Poll[3] for attachment-line transition at supersonic speeds is defined by $\bar{R}^* = V_{es}\eta^*/\nu^*$. Here, η^* is the local length scale as follows:

$$\eta^* = \sqrt{\frac{D}{U_\infty}\left[\nu^* \Big/ \left(\frac{D}{U_\infty}\frac{du_e}{dx}\right)_{x=0}\right]} \tag{3}$$

where ν^* is the kinematic viscosity evaluated at the reference temperature T^* that is defined by $T^* = T_{es} + 0.10(T_w - T_{es}) + 0.60(T_r - T_{es})$. $\bar{R}^*$ can also be expressed with ReD as follows:

$$\bar{R}^* = \sqrt{ReD} \times \sqrt{\left[\sin\Lambda \tan\Lambda \Big/ \left(\frac{D}{U_\infty}\frac{du_e}{dx}\right)_{x=0}\right]} \times \sqrt{\frac{\nu_\infty}{\nu^*}} \tag{4}$$

Crossflow Parameter

The crossflow Reynolds number has been used for the correlation of off-attachment-line transition data due to crossflow instability.[3] The definition of this parameter is $\chi = w_{max}\Delta/\nu_e$, where w_{max} is the maximum value of the crossflow velocity and Δ is the normal distance from the surface to the point where the crossflow velocity reduces to 1% of w_{max}. In the present study, this parameter is calculated from the following equation according to Chapman's method[10]:

$$\chi = \sqrt{ReD}\sqrt{\left[\frac{\nu_{es}}{\nu_\infty} \Big/ \cos\Lambda\left(\frac{D}{U_\infty}\frac{du_e}{dx}\right)_{x=0}\right]}$$

$$\times H\beta_{max} \int_0^{\zeta_{0.01\beta_{max}}} h\,d\zeta \tag{5}$$

where $H = (Q_e/\nu_e)/(Q_\infty/\nu_\infty)$ is the ratio of the local Reynolds number to the freestream one. Also $\beta_{max} = w_{max}/Q_e$ is the ratio of the maximum crossflow velocity and $\int h\,d\zeta$ is the static enthalpy integral that can be obtained by laminar boundary-layer theory.

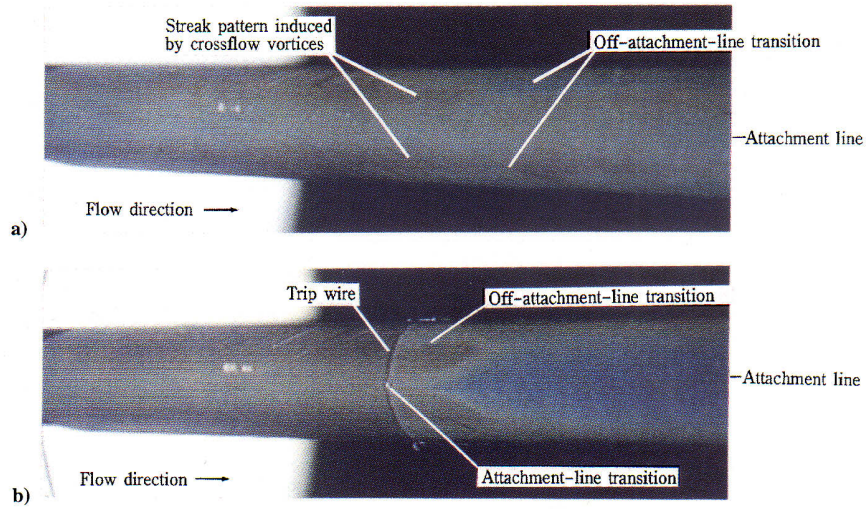

Fig. 4 Visualization of transition near the leading edge of a swept cylinder with the liquid-crystal technique ($M_\infty = 5.0$, $\Lambda = 45$ deg, $ReD = 1.0 \times 10^6$) a) without end plates and trip wires and b) with a trip wire; $d = 0.05$ mm, $d/\eta^* = 1.0$, $s_{trip}/D = 5$.

Results and Discussion

Flow Visualization

Figure 4 shows typical results of liquid-crystal visualizations. The sweep angle is $\Lambda = 45$ deg, the freestream Mach number is $M_\infty = 5.0$, and the freestream Reynolds number based on the cylinder diameter is $ReD = 1.0 \times 10^6$, which corresponds to $Re\theta = 350$ and $\bar{R}^* = 680$. Figures 4a and 4b are for the cylinder without contaminations, i.e., without end plates and trip wire, and for small trip wire disturbances (the diameter of the trip wire is $d = 0.05$ mm), respectively.

In Fig. 4a, the attachment layer is laminar along the entire attachment line, but at the locations off the attachment line, the high heating region can be observed that means the occurrence of boundary-layer transition. In the region upstream of the transition front, fine streak pattern indicating the formation of streamwise vortices due to crossflow instability can be seen. The transition process off the attachment line at hypersonic speeds is similar to the subsonic one due to crossflow instability. The wave length of the vortices measured at the angular coordinate of $\theta = 30$ deg is approximately $\lambda = 1.2$ mm of which the ratio to the attachment-layer thickness is $\lambda/\delta_s = 5.7$.

In Fig. 4b, the color of the liquid crystals changes abruptly from brown to blue at the location of the trip wire, indicating attachment-line transition caused by the trip wire. Downstream of the trip wire, the boundary layer on the entire surface of the cylinder becomes turbulent. The off-attachment-line transition and the fine streak pattern upstream of the transition front can be observed in the same manner as in Fig. 4a.

When the end plate was attached, the attachment layer was either laminar or turbulent along the entire attachment line, depending on freestream Reynolds number, and the attachment-line transition at the midspan could not be observed at the present test conditions.

Transition on the Attachment Line

Comparison with Previous Criteria

The present data for the attachment-line transition with and without end plates were compared with criteria of Bushnell and Huffman[4] and Poll.[1-3] These criteria are summarized in Table 2. Figure 5 shows the present data at $M_\infty = 5.0$ and 6.9 as plots of the freestream Reynolds number at transition $(ReD)_t$ vs the spanwise Mach number M_{es}. In this figure the transition data at $M_\infty = 3.5$ obtained by Creel et al.[5] are also shown. The attachment-line transition with end plate disturbances occurred at $ReD = 0.15$–0.33×10^6, which was roughly in agreement with the Bushnell and Huffman[4] criterion for large upstream disturbances. When the end plates were removed, the attachment layers remained laminar up to $ReD = 1.0 \times 10^6$ and 0.9×10^6 at $M_\infty = 5.0$ for $\Lambda = 45$ and

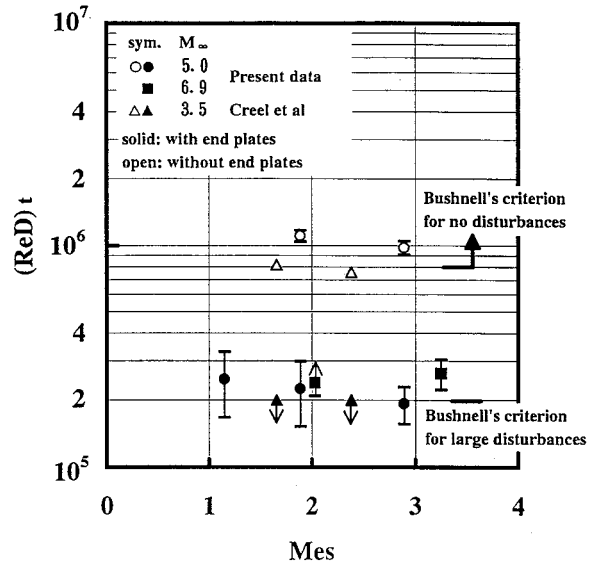

Fig. 5 Freestream Reynolds number based on the cylinder diameter at attachment-line transition with and without end plate disturbances.

60 deg, respectively. These values are within the range of Ref. 4 criterion for no contamination, but higher than those of the Creel et al.[5] data at $M_\infty = 3.5$, in spite of a certain surface roughness due to the liquid-crystal coating.

The present results for the attachment-line transition are again summarized in Fig. 6 as plots of the local momentum thickness Reynolds number at transition $(Re\theta)_t$ vs M_{es}. Poll's criteria, $\bar{R}^* = 245$ for large upstream disturbances and $\bar{R}^* = 650$ for no disturbances, are also shown in the range of $T_{tu}/T_r = 0.6$–0.9 that corresponds to the present test conditions. The trend that $(Re\theta)_t$ increases with M_{es} is qualitatively in agreement with Poll's criteria. But the values with end plates are larger at higher M_{es}, than those due to Poll's criterion for large upstream disturbances. Plots of the transition local length scale Reynolds number with end plates $(\bar{R}^*)_t$ vs M_{es} are shown in Fig. 7 together with previous data.[11] In general, experimental data is usually correlated with $\bar{R}^*$. As mentioned before, however, the present data is obviously larger than those due to Poll's criterion and other experimental data. The present data represents the upper boundary of transition Reynolds number because the liquid-crystal flow visualization can detect the end of transition, i.e., fully turbulent boundary layer, but not the onset of transition, e.g., turbulent burst. Therefore, the present data may have been higher

Table 2 Previous criteria for attachment-line transition at super-/hypersonic speeds

Reference	Contamination	M_∞	Λ, deg	Criteria
Bushnell and Huffman[4]	large	~9.8	~82	$ReD = 0.2 \times 10^6$
	none	~8	~78	$ReD > 0.8 \times 10^6$
Poll[3]	large	——	——	$\bar{R}^* = 245$
	none	——	——	$\bar{R}^* \geq 650$

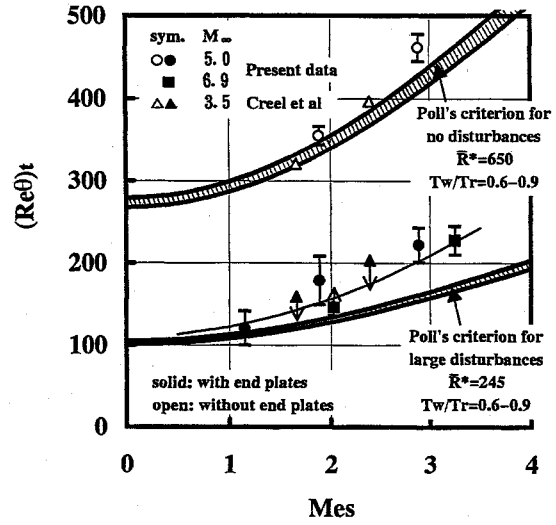

Fig. 6 Local momentum thickness Reynolds number at attachment-line transition vs spanwise Mach number.

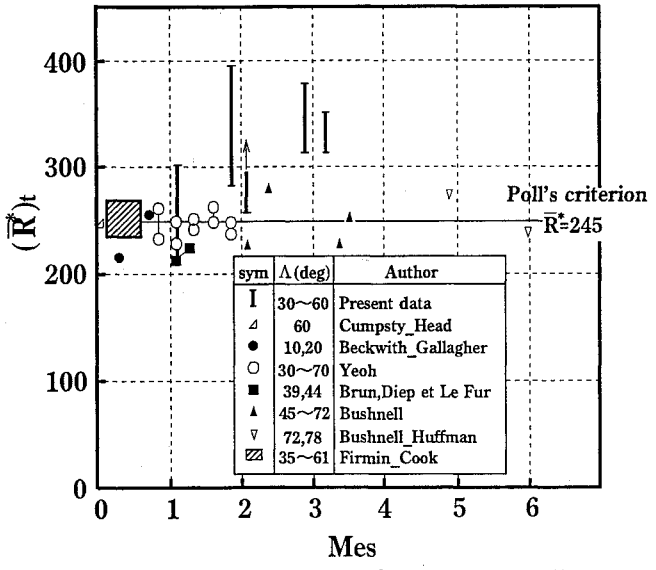

Fig. 7 Comparison with Poll's criterion[3] and previous data[11] for large upstream disturbances.

than Poll's criterion that represents the onset of transition. It should be also noted, however, that in the present test conditions the initial disturbances generated in the vicinity of the end plate/cylinder junction may be smaller because the boundary layer on the end plate is expected to be laminar.

Effects of Surface Roughness Height

Figure 8 shows the effect of the surface roughness height due to trip wires on the attachment-line transition Reynolds number as plots of $(\bar{R}^*)_t$ vs the normalized roughness height d/η^*. In this figure, the present data for the cases without end plates and trip wires are plotted at $d/\eta^* = 0.2$–0.3 corresponding to the roughness height due to the liquid-crystal coating. Trends of $(\bar{R}^*)_t$ with d/η^* are generally similar to those of the Creel et al.[5] data at $M_\infty = 3.5$ with respect to the critical roughness height where $(\bar{R}^*)_t$ is abruptly reduced

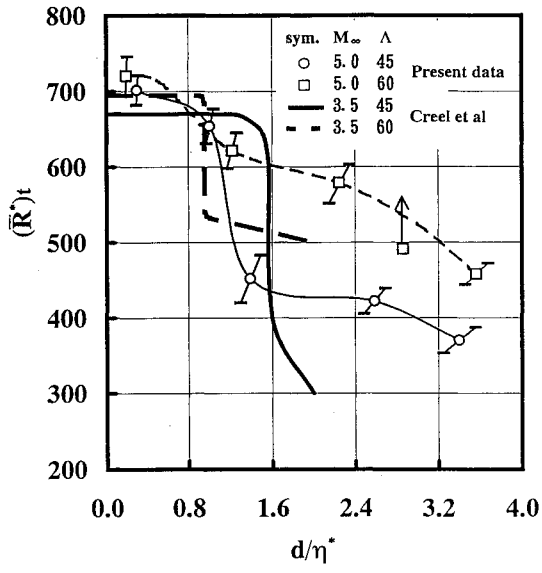

Fig. 8 Variation of attachment-line transition Reynolds number with normalized surface roughness height.

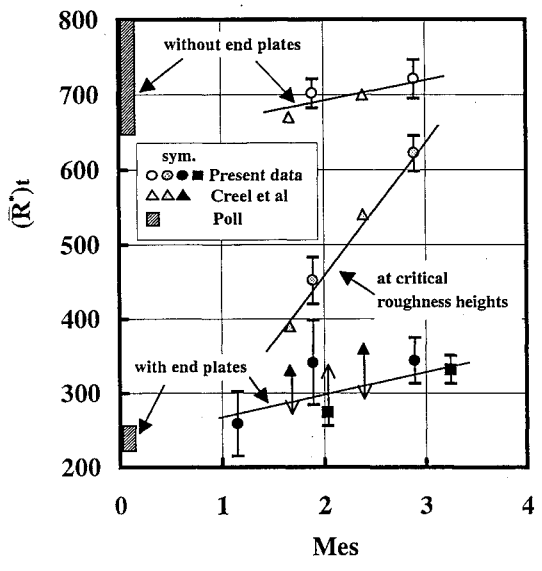

Fig. 9 Effects of spanwise Mach number on attachment-line transition Reynolds number.

as the roughness height increases. The critical roughness height as $(d/\eta^*)_{crit}$ =1.0–1.4 for $\Lambda = 45$ deg at $M_\infty = 5.0$ where $(\bar{R}^*)_t$ is reduced from 660 to 450. For $\Lambda = 60$ deg, the critical roughness height could not be determined exactly in the present experiments, but it can be expected to be $0.2 < (d/\eta^*)_{crit} < 1.2$, where $(\bar{R}^*)_t$ decreases from 720 to 620. And the Creel et al.[5] data at $M_\infty = 3.5$ show that $(\bar{R}^*)_t$ at the critical roughness height changes from 680 to 390 for $\Lambda = 45$ deg and from 700 to 540 for $\Lambda = 60$ deg. These results show that the change of $(\bar{R}^*)_t$ at the critical roughness height depends strongly on Λ and M_∞, i.e., on M_{es}, and it is smaller at higher M_{es}. For subcritical roughness heights, present values of $(\bar{R}^*)_t$ are approximately $(\bar{R}^*)_t$ = 680–750, which generally agree with the Creel et al.[5] data and subsonic data of Refs. 1–3. $(\bar{R}^*)_t$ at supercritical roughness heights, however, depends strongly on Λ and M_∞, i.e., on M_{es}. $(\bar{R}^*)_t$ in the region of supercritical roughness heights is larger at higher M_{es}, and even at $d/\eta^* = 3.5$, approximately corresponding to the attachment-layer thickness, the values are higher than those for the end plate disturbances. Consequently, an asymptotic value of $(\bar{R}^*)_t$ with large roughness heights due to trip wires was not obtained in the present investigation.

Effects of Spanwise Mach Number

Figure 9 shows $(\bar{R}^*)_t$ plotted against M_{es} for the cylinder with and without end plates and at the critical roughness height. For the end

plate disturbances, $(\bar{R}^*)_t$ increases slightly with M_{es}, and the values at higher M_{es} are somewhat larger than those due to Poll's criterion.[3] This trend can also be observed for the cylinder without end plates. But the change of $(\bar{R}^*)_t$ with M_{es} is relatively small. It is, therefore, concluded that $\bar{R}^*$ can potentially correlate the transition data for no and large upstream disturbances over a wide range of Mach numbers. On the other hand, the value of $(\bar{R}^*)_t$ at the critical roughness height increases rapidly from 380 to 620 as M_{es} increases from 1.66 to 2.89 and is close to the subcritical one at higher M_{es}. Although there are only few data, it is concluded that the spanwise Mach number is an important parameter for the occurrence of attachment-line transition due to the surface roughness.

Transition Off the Attachment Line

Transition at the locations off the attachment line could be observed at $ReD \geqq 1.0 \times 10^6$ and 0.9×10^6 at $M_\infty = 5.0$ for $\Lambda = 45$ and 60 deg, respectively, at $M_\infty = 5.0$. As shown in Fig. 4a, a fine streak pattern could be observed upstream of the transition front that indicates the occurrence of streamwise vortices due to crossflow instability. The process of the off-attachment-line transition at super-/hypersonic speeds is fundamentally similar to the transition process at subsonic speeds confirmed in previous work.

The location of the transition front for $\Lambda = 45$ deg moved upstream from the angular coordinate of $(\theta)_t = 40$ to 35 deg as the Reynolds number increased from $ReD = 1.0 \times 10^6$ to 1.2×10^6. The value of the crossflow Reynolds number at transition was approximately $(\chi)_t = 380$ independent of the freestream Reynolds number. For $\Lambda = 60$ deg at $M_\infty = 5.0$, however, the value was about $(\chi)_t = 650$, i.e., the crossflow Reynolds number at transition depended strongly on the sweep angle. But except for the present data, there are no available data for the off-attachment-line transition at hypersonic speeds as far as the authors know. Further investigations are required to identify the effects of sweep angle and Mach number.

Concluding Remarks

Boundary layer transition data were obtained from flow visualizations by the liquid-crystal technique on three swept cylinders with and without end plates and sweep angles of 30, 45, and 60 deg, respectively, at freestream Mach numbers of 5.0 and 6.9. Also investigated was the response of attachment-line transition to surface roughness heights due to trip wires. These transition data were compared with previous data. Following are some remarks resulting from the present study.

1) Transition on the attachment line of swept cylinders occurred at freestream Reynolds numbers, based on the diameter of the cylinder, of approximately $0.15–0.33 \times 10^6$ and $0.9–1.2 \times 10^6$ with and without end plates, respectively. The transition Reynolds numbers agree reasonably well with those due to criteria of Bushnell and Huffman.[4]

2) At the present test conditions, the local Reynolds number at attachment-line transition increases slightly as the spanwise Mach number increases, so that the attachment-line transition data for the cylinder with and without large disturbances can potentially be correlated with the local length scale Reynolds number.

3) Trends in the dependence of the local transition Reynolds number on the normalized surface roughness height are generally similar to the ones observed by Creel et al.[5]: there is a critical roughness height where the transition Reynolds numbers rapidly decrease as the roughness height increases. Behavior of the transition Reynolds numbers around the critical roughness height strongly depends on the spanwise Mach number.

4) With flow visualizations by the liquid-crystal technique, transition at the locations off the attachment line could be observed at freestream Reynolds numbers of about 1.0×10^6 and 0.9×10^6 for sweep angles of 45 and 60 deg, respectively, at the freestream Mach number of 5.0. In the laminar flow region upstream of the transition front, fine streaks could be observed, confirming the existence of streamwise vortices possibly induced by crossflow instability at hypersonic speeds.

5) Crossflow Reynolds numbers at off-attachment-line transition depended strongly on sweep angles, and the values were about 380 and 650 for the sweep angles of 45 and 60 deg, respectively, at a freestream Mach number of 5.0.

Acknowledgments

The authors wish to thank L. Budke and D. Haßbargen for their technical assistance with wind tunnel operation and preparation of the experiments. The authors also would like to thank H. Schöler for his suggestions concerning the liquid-crystal technique.

References

[1]Poll, D. I. A., "Leading Edge Transition on Swept Wings," AGARD-CP-224, 1977, pp. 21-1–21-11.

[2]Poll, D. I. A., "Three-Dimensional Boundary Layer Transition via the Mechanisms of Attachment Line Contamination and Cross Flow Instability," *Proceedings of IUTAM Symposium on Laminar-Turbulent Transition* (Stuttgart, Germany), Springer–Verlag, Berlin, 1979, pp. 253–362.

[3]Poll, D. I. A., "Transition Description and Prediction in Three-Dimensional Flows," AGARD-Rept. 709, June 1984, pp. 5-1–5-23.

[4]Bushnell, D. M., and Huffman, J. K., "Investigation of Heat Transfer to a Leading Edge of a 76 Swept Fin With and Without Chordwise Slots and Correlations of Swept-Leading-Edge Transition Data for Mach 2 to 8," NASA TMX-1475, Dec. 1967.

[5]Creel, T. R., Jr., Beckwith, I. E., and Chen, F. J., "Transition on Swept Leading Edges at Mach 3.5," *Journal of Aircraft*, Vol. 24, No. 10, 1987, pp. 710–717.

[6]Arnal, D., Vignau, F., and Juillen, J. C., "Boundary Layer Tripping in Supersonic Flow," *Proceedings of IUTAM Symposium on Laminar-Turbulent Transition* (Toulouse, France), Springer–Verlag, Berlin, 1989, pp. 669–679.

[7]Ludwieg, H., Hottner, T., and Grauer-Carstensen, H., "Der Rohrwindkanal der Aerodynamichen Versuchsanstalt Göttingen," *Jahrbuch 1969 der DGLR*, DGLR, Göttingen, Germany, 1969, pp. 52–58.

[8]Wendt, V., Kreplin, H., Höhler, G., Grosche, F., Krogmann, P., and Simen, M., "Planar and Conical Boundary Layer Stability Experiments at Mach 5," AIAA Paper 93-5112, Nov. 1993.

[9]Schöler, H., "Thermal Imaging on Missiles in Hypersonic Flow," AGARD-CP-493, 1990, pp. 29-1–29-A3.

[10]Chapman, G. T., "Some Effects of Leading-edge Sweep on Boundary-Layer Transition at Supersonic Speeds," NACA-TN-D-1075, Sept. 1961.

[11]Arnal, D., "Laminar-Turbulent Problems in Supersonic and Hypersonic Flows," AGARD-R-761, June 1989, pp. 8-1–8-45.

Color reproduction courtesy of National Aerospace Laboratory, Japan